Multiphase region of helimagnetic superlattices at low temperature in an extended six-state clock model



2006 J. Phys. A: Math. Gen. 39 5681

(http://iopscience.iop.org/0305-4470/39/20/004)

INSTITUTE OF PHYSICS PUBLISHING JOURNAL OF PHYSICS A: MATHEMATICAL AND GENERAL

J. Phys. A: Math. Gen. **39** (2006) 5681–5694 doi:10.1088/0305-4470/39/20/004

# Multiphase region of helimagnetic superlattices at low temperature in an extended six-state clock model

**D C Lovelady, H M Harper, I E Brodsky[1] and D A Rabson**

Department of Physics, PHY 114, University of South Florida, 4202 East Fowler Avenue, Tampa, FL 33620, USA

E-mail: davidra@ewald.cas.usf.edu

Received 31 December 2005, in final form 14 March 2006
Published 3 May 2006
Online at stacks.iop.org/JPhysA/39/5681

**Abstract**

The variety of magnetic phases observed in rare-earth heterostructures at low temperatures (Jehan *et al* 1993 *Phys. Rev.* B **48** 5594–606), such as Ho/Y, may be elucidated by an ANNNI-like model Hamiltonian. In previous work modelling bulk Ho (Seno, Rabson and Yeomans 1993 *J. Phys. A: Math. Gen.* **26** 4887–905), such a Hamiltonian with a one-dimensional parameter space produced a single multiphase point. In contrast, the parameter space of the heterostructure model is three dimensional, and instead of an isolated multiphase point, we find two-dimensional multiphase regions. In an example of Villain's 'order from disorder' (Villain, Bidaux, Carton and Conte 1980 *J. Physique* **41** 1263–72; Pimpinelli, Uimin and Villain 1991 *J. Phys.: Condens. Matter* **3** 4693–719), an infinitesimal temperature breaks the ground-state degeneracy. In first order of a low-temperature expansion, we find that the degeneracy is broken everywhere in a multiphase region except on a line. A segment of the line appears to remain multiphase to all orders in a low-temperature expansion when the number $L$ of magnetic layers between non-magnetic spacers is 4 but not for other values of $L$. For $L = 4$, the hierarchy of phases more closely resembles that in the ANNNI model than in the bulk six-state clock model on which the present model is based.

PACS numbers: 64.60.Cn, 05.50.+q, 75.70.Cn

## 1. Introduction

Layered planes of rare-earth metals exhibit a wealth of magnetically-ordered phases at low temperature. In helimagnetic phases, spins (treated classically) align ferromagnetically within each plane, with an axial RKKY interaction responsible for a progression of spin angles through successive planes [5, 6]. Strong easy-axis anisotropy may frustrate the natural RKKY

[1] Current address: Department of Mathematics, University of Florida, Gainesville, FL, USA.

  

pitch angle, leading to a multitude of possible phases characterized by the number of layers separating skips, or 'walls,' in the pattern of pitch angles. In the axial-next-nearest-neighbour Ising (ANNNI) [7–10] and related clock models [2, 11–15], a single parameter controls the relative strengths of competing interactions, and at a single value of this parameter, infinitely many phases coexist; this is called a multiphase point. Since these phases cover all allowed spacings between walls, such phases are indistinguishable from random sequences. Thus the zero-temperature state is disordered. This disorder is broken at infinitesimal temperature in an example of 'order from disorder' [3, 4]. We now ask what happens in a model of helimagnetic heterostructures with a three-dimensional parameter space: we identify fully two-dimensional multiphase regions and investigate the topology of the low-temperature phase diagram.

With the giant magnetoresistive effect [16] in ferromagnetic/nonmagnetic superlattices having spawned important technological applications that reached the market around 1997 [17, 18], it seems practical, as well as theoretically interesting, to examine the possible phases of helimagnetic/nonmagnetic superlattices. Such superlattices have been deposited using molecular-beam epitaxy, alternating dysprosium [19], erbium [20], or holmium [1] with non-magnetic yttrium spacer layers as well as holmium with lutetium [21]. Surprisingly, neutron-scattering experiments show that the helicity of the spins in the rare-earth layers is preserved across the spacers, with the magnetic moments forming long-period 'spin-slip' phases [1]. RKKY-like polarization [22] of conduction electrons in the non-magnetic layers is again implicated [23, 24]; in any case, we can model the indirect exchange across non-magnetic spacers in parallel with that between successive magnetic planes. If the exchange parameters can be controlled with pressure, external fields, or spacer-layer thickness, such systems could possibly be useful as magnetic sensors or in data-storage applications. Axially modulated, high-order, commensurate phases are not limited to rare-earth heterostructures: Szpilka and Fisher [9] cite half a dozen other systems in which such phases have been observed, ranging from CeSb [25] to ferroelectric thiourea [26, 27].

Seno *et al* [2] applied the ANNNI ideas to a case of infinite hexagonal anisotropy, the six-state clock model, relevant, for example, to bulk holmium[2]. A spin $\alpha$ in the $j$th plane points in a direction that is an integral multiple, $n_{j\alpha}$, of $2\pi/6$. At zero temperature, all the spins in a plane point in the same direction $(n_j)$, and the model is controlled by a single parameter, the ratio $x$ of the strength of the next-nearest-axial-neighbour antiferromagnetic $(J_2)$ to nearest-axial-neighbour ferromagnetic $(J_1)$ interaction, with the axial terms in the Hamiltonian summing $-J_1\cos(2\pi(n_{j+1,\alpha}-n_{j,\alpha})/6)$ and $+J_2\cos(2\pi(n_{j+2,\alpha}-n_{j,\alpha})/6)$. For $0 < x < 1/3$, the ground state is a ferromagnet, for $1/3 < x < 1$ a helimagnet with no walls, and for $x > 1$ a helimagnet interrupted by walls every second layer. At the single point $x = 1$ in the one-dimensional phase diagram, infinitely many phases coexist in the ground state. We represent the helimagnetic phase $(1/3 < x \leqslant 1)$ by the axial sequence $\ldots 012345012\ldots$, understanding that this includes as well the translations and reflections of the sequence. The two coexisting period-2 phases for $x > 1$ are represented by $\ldots 00330033\ldots$ and $\ldots 01|34|01|34\ldots$: this last is thought of as a modification of the helical phase by the insertion of skips, or walls (denoted '|'), every second layer. The walls are analogous to domain walls in the ANNNI model. At the multiphase point, $x = 1$, in addition to $\ldots 00330033\ldots$, a helical phase with walls placed anywhere at least two layers apart is a ground state of the system, e.g., $\ldots 01|345|12|450\ldots$. A convenient notation in ANNNI-type models labels a periodic phase by the spacings between successive walls: thus, this last example is $\langle 23\rangle$, the phase with walls every second layer $\langle 2\rangle$, and the bare helical phase without walls $\langle\infty\rangle$. In a low-temperature expansion, Seno *et al*

[2] An extension of this work presented a small-inverse-anisotropy expansion about the clock model and again found a hierarchy of phases emanating from the multiphase point at infinite anisotropy [28].

followed a hierarchy of phases (similar to what we describe below) and showed that each phase between $\langle 23 \rangle$ and $\langle \infty \rangle$ acquires a region of stability at infinitesimal temperature.

The forgoing model simplifies the actual magnetic structure of bulk holmium. Neutron scattering gives the turn angle per atomic layer as 30° rather than 60°, with moments bunched in pairs around the six easy axes [29, 1], and while the average turn angle increases in films, the effect is thought to be due to interspersal of singlets among the pairs; thus the $\langle 3 \rangle$ phase in the simplified model might actually represent moments . . . 00122344 . . ., where pairs of repeated spins lie a few degrees before and after the easy-axis direction (see figure 14 of [1]). The model, or its present extension to superlattices, was meant not to reproduce realistic details of a particular rare-earth helimagnet but rather to reduce a system with competing crystal-field and exchange interactions to the simplest form, in which exact results are possible, so as to investigate universal properties of the resulting hierarchy of commensurate, longitudinally-modulated spin-slip phases.

## 2. The model and its ground states

We consider a superlattice in which blocks of $L$ magnetic layers are separated by non-magnetic spacers characterized by effective couplings $J_1'$ and $J_2'$; this simple extension of the bulk model of [2] gives the full Hamiltonian

$$\begin{aligned}\mathcal{H} = -\frac{1}{2}J_0 \sum_{i,\alpha,\beta(\alpha)} \cos\left(\frac{2\pi}{6}(n_{i\alpha} - n_{i\beta})\right) \\ - J_1 \sum_{i,\alpha} \cos\left(\frac{2\pi}{6}(n_{i\alpha} - n_{i+1,\alpha})\right) + J_2 \sum_{i,\alpha} \cos\left(\frac{2\pi}{6}(n_{i\alpha} - n_{i+2,\alpha})\right) \\ - J_1' \sum_{i,\alpha}{}' \cos\left(\frac{2\pi}{6}(n_{i\alpha} - n_{i+1,\alpha})\right) + J_2' \sum_{i,\alpha}{}' \cos\left(\frac{2\pi}{6}(n_{i\alpha} - n_{i+2,\alpha})\right), \qquad (1)\end{aligned}$$

where $i$ labels layers, $\alpha$ a spin within a (simple-hexagonal) layer and $\beta(\alpha)$ its nearest neighbours. The unprimed sums in the second line are taken only over bonds that do not straddle a non-magnetic spacer, while the primed sums in the third line are taken only over bonds that do. For purposes of the low-temperature expansion, the in-plane ferromagnetic coupling constant $J_0$ is taken to be positive and much stronger than any of the axial couplings [2]. Since we are looking for helical phases, we take all of the remaining four couplings also to be positive. (Certain negative couplings are in fact related to the positive sector by symmetries of $\mathcal{H}$.) The model reduces to that of [2] when $J_1' = J_1$ and $J_2' = J_2$ or, equivalently, when $L = 1$. The three-dimensional coupling space is given by $x = J_2/J_1$, $y = J_1'/J_1$ and $z = J_2'/J_1$; it is convenient to set $J_1 = 1$.

We generalize the previous notation to accommodate states of a superstructure in which blocks of $L$ magnetic layers are separated by non-magnetic spacers, denoted by $\|$, with the arrangement repeated periodically. (The symbol $\|$ may denote any number of atomic layers of the non-magnetic metal.) Since the direct interactions in (1) extend a maximum of two layers in the axial direction, walls are classified in three categories. A wall at least two layers from a spacer has the same energy cost as in the bulk model and is termed a type-1 wall, for example ($L = 5$)

$$\ldots \| 0123 | 50 \| 12 \ldots . \qquad (2)$$

Insertion of a wall one layer from a non-magnetic spacer has a different energy cost, since a $J_2'$ bond is broken. This is termed a type-2 wall:

$$\ldots \| 01234 | 0 \| 12 \ldots . \qquad (3)$$

A type-3 wall coincides with a non-magnetic spacer:

$$\ldots \| 012345 \| | 12 \ldots . \tag{4}$$

Helical configurations, including $\langle\infty\rangle$ itself, that differ from $\langle\infty\rangle$ only by the insertion of walls are called wall states. These states preserve the sense of helicity (positive or negative). We consider $L \geqslant 3$, as $L = 1$ is the same as bulk, while $L = 2$ omits the $J_2$ $(x)$ parameter and so has only a two-dimensional parameter space. It is also less likely to be of experimental interest.

A straightforward calculation yields the total energy of a wall state as a function of the densities $W_i$ of walls of the three types:

$$E_{\text{wall}} = -\frac{1}{2L}((1+x)(L-2)+1+y+2z)+(1-x)W_1+\left(1-\frac{x+z}{2}\right)W_2+(y-z)W_3. \tag{5}$$

As in the original model, successive walls are energetically forbidden. We seek regions of the three-dimensional parameter space in which the insertion of a wall of some type costs no energy: this occurs when the coefficient of one or more of the densities $W_i$ vanishes. Thus the planes $x = 1$, $(x+z)/2 = 1$ and $y = z$ all potentially constitute multiphase regions; however, it is also necessary to consider competing non-wall states, which may have lower energies. For present purposes, we shall concentrate on the $y = z$ plane, for which type-3 walls cost no energy. Since a negative energy for type-2 walls would shut type-3 walls out, we examine the part of the $y = z$ plane to the left of the $x + z = 2$ line. By considering points to the left of the line $x = 1$, we exclude type-1 walls as well. For $L = 4$, direct calculation gives the phase diagram of figure 1. An exhaustive computer search (of phases of length $3L = 12$ with twisted periodic boundary conditions) verified that the wall-state energy (5) is lower than that of any competing phase inside a triangle in the $y = z$ plane, which constitutes a multiphase region. Comparable wall-state regions were calculated numerically for $L$ in the range 3–11.

Since we are concentrating on a region in which type-1 and type-2 walls are excluded, while type-3 walls cost no energy, we adapt the notation of [2] to count magnetic blocks, rather than magnetic layers, between walls. Thus, for example, with $L = 4$, $\langle 1\rangle$ has a wall coinciding with each spacer, while the $\langle 2\rangle$ phase has a wall at every other spacer. Since no restriction prevents adjacent walls of this type, the count of possible phases is simply 2 to the power of the number of magnetic blocks; this represents a simplification relative to the ANNNI and other related models [30].

## 3. Low-temperature expansion: first order

The novel feature presented by the current problem is the multiphase triangle (for $L = 4$ or a similar polygon for other $L$) throughout which infinitely many phases coexist at zero temperature. An interesting theoretical question is how thermal disorder can distinguish the free energies of all these phases in the given region.

Although the Hamiltonian (1) contains only first- and second-neighbour axial terms, a non-zero temperature introduces effective long-range interactions through an axial chain of thermally-excited spins, each pointing in a direction at variance with its in-plane neighbours [7, 8, 2]. By analogy to the ANNNI model, we call such excitations 'spin flips.' Since the number of ways an excitation of a particular energy may occur depends on the state, flipped spins provide an entropic mechanism for distinguishing the free energies of wall states at infinitesimal temperature. If the $i$th excitation, which may involve several spins,

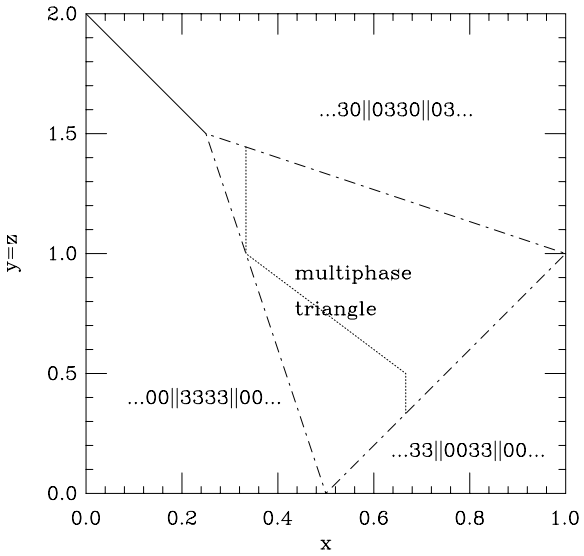


**Figure 1.** Ground-state phase diagram for (part of) the $y = z$ plane, $L = 4$. The horizontal axis gives the normalized bulk second-neighbour coupling, the vertical the couplings across non-magnetic spacers. Outside the triangle delimited by dot-dashed lines, the ground states are as indicated. Inside the triangle, wall states are the ground states. (An exhaustive search found no lower-energy states of length up to $3L$.) Similar ground-state phase diagrams were calculated for other values of $L$. The first-order low-temperature expansion gives $\langle\infty\rangle$ to the left of the dotted line within the triangle and the $\langle 1\rangle$ phase to the right; on the line itself, these phases and their progeny coexist, requiring a higher-order low-temperature expansion to distinguish. On roughly the upper half of the left leg of the dotted line, from $z = 11/9$ to $z = 13/9$, we believe infinitely many phases of the form $\langle 1^k 2\rangle$ coexist to all orders.

has an energy $\Delta E_i$ relative to the ground-state energy per spin $E_0$ and can be placed on the lattice of $N$ spins $g_i$ different ways, the free energy per spin is given by the linked-cluster theorem [31]:

$$f = E_0 - k_B T \sum_i \gamma_i \mathrm{e}^{-\beta \Delta E_i}, \tag{6}$$

where $\gamma_i = \lim_{N\to 0} g_i/N$ is the intensive part of $g_i/N$. (The limit discards those terms in $g_i$ that go as higher powers of $N$; such terms come from independent clusters of spin excitations.)

We apply the method first to an isolated spin flip, which may occur in a layer adjacent to or one layer separated from a spacer, or it may ($L > 4$) occur in bulk. An isolated spin flip in bulk gives the same contribution to $f$ regardless of phase, so we calculate the energies and counts $\gamma_i$ just for the first two cases, leading to the weights in table 1. The case $L = 3$ requires special treatment because the cost of an excitation in the layer in the middle of a block depends on the presence or absence of walls on both sides.

We consider $L \geqslant 4$ first. If there are no type-3 walls, the only single-spin excitations (other than bulk) will be of one of the types in the first two rows of table 1. This describes the $\langle\infty\rangle$ phase. If a phase has the maximum density of type-3 walls, the excitations will be of the types in the second two rows. This is the $\langle 1\rangle$ phase. To this first order in the low-temperature expansion, any other wall phase (e.g., $\langle 2\rangle$) will have a free energy intermediate between these two cases. Thus we look first for the coexistence of $\langle 1\rangle$ and $\langle\infty\rangle$. Subtracting rows 1

**Table 1.** Contributions to (6) are formed by a count (per spin) of the number of ways of forming the excitation times a Boltzmann factor. The left column gives an example of the excitation under consideration, where the caret ($\wedge$) marks the plane in which a single spin is rotated ('flipped') plus 60° or minus 60° from the angle of its neighbours in the plane. The second column gives the Boltzmann factor, and the remaining columns give the intensive counts $\gamma_i$ weighting the Boltzmann factor for the cases $\langle 1\rangle$, $\langle 2\rangle$ and $\langle\infty\rangle$. $L$ is the number of magnetic layers in a block. The last three rows apply only to $L = 3$. Here, $\beta$ is the inverse temperature, $q = \exp(-\beta J_0/2)$, $t[=6]$ the number of in-plane nearest neighbours and $r = \exp(-\beta J_1/2)$.

| | | | Intensive count | | |
|---|---|---|---|---|---|
| | Excitation | Boltzmann factor | $\langle 1\rangle$ | $\langle 2\rangle$ | $\langle\infty\rangle$ |
| 1 | $45\hat{0}1\,\|\,23$ | $q^t(r^{1-x+2z} + r^{1+2x-z})$ | 0 | $1/L$ | $2/L$ |
| 2 | $450\hat{1}\,\|\,23$ | $q^t(r^{2-x-y+2z} + r^{-1+2x+2y-z})$ | 0 | $1/L$ | $2/L$ |
| 3 | $45\hat{0}1\,\|\,\|\,34$ | $q^t(r^{1-x+z} + r^{1+2x+z})$ | $2/L$ | $1/L$ | 0 |
| 4 | $450\hat{1}\,\|\,\|\,34$ | $q^t(r^{2-x-2y+z} + r^{-1+2x+y+z})$ | $2/L$ | $1/L$ | 0 |
| 5 | $0\,\|\,1\hat{2}3\,\|\,4$ | $2q^t r^{1+z}$ | 0 | 0 | $1/L$ |
| 6 | $0\,\|\,\|\,2\hat{3}4\,\|\,5$ | $q^t(r + r^{1+3z})$ | 0 | $1/L$ | 0 |
| 7 | $0\,\|\,\|\,2\hat{3}4\,\|\,\|\,0$ | $2q^t r^{1+2z}$ | $1/L$ | 0 | 0 |

and 2 from the sum of rows 3 and 4 gives the free–energy difference

$$\begin{aligned}\Delta f &= f_{\langle 1\rangle} - f_{\langle\infty\rangle} \\ &= -\frac{2}{L}k_B T q^t (r^{1-x+z} + r^{1+2x+z} + r^{2-x-2y+z} + r^{-1+2x+y+z} \\ &\quad - r^{1-x+2z} - r^{1+2x-z} - r^{2-x-y+2z} - r^{-1+2x+2y-z}),\end{aligned} \tag{7}$$

where $\beta = 1/(k_B T)$ is the inverse temperature, $t$ is the number of in-plane nearest neighbours, $q = \exp(-\beta J_0/2)$ and $r = \exp(-\beta J_1/2)$. Setting $\Delta f = 0$ and $y = z$ yields the expression

$$r^{3x} = \frac{r^z + r - 1 - r^{1-2z}}{1 + r^{z-2} - r^{-2z} - r^{-2}}. \tag{8}$$

In the zero-temperature limit, $r \to 0$, so the power of $r$ with the smallest exponent dominates. This allows us to solve for the coexistence line,

$$x = \begin{cases} \frac{2}{3} & \text{for} \quad 0 < z \leqslant \frac{1}{2} \\ 1 - \frac{2}{3}z & \text{for} \quad \frac{1}{2} \leqslant z \leqslant 1 \\ \frac{1}{3} & \text{for} \quad 1 \leqslant z \leqslant 2 \end{cases} \qquad (L \geqslant 4), \tag{9}$$

drawn as a dotted line in figure 1. In the multiphase region to the left of this line, the $\langle\infty\rangle$ phase has the lowest free energy, breaking the infinite degeneracy of zero temperature[3]. To the right of the line, the $\langle 1\rangle$ phase dominates. On the line itself, all wall phases remain degenerate; to break the degeneracy it will be necessary to consider more flipped spins.

First, however, the model with $L = 3$ introduces a new element to the low-temperature expansion. In the last three rows of table 1, the count of the $\langle 2\rangle$ phase does not merely interpolate between the counts of $\langle 1\rangle$ and $\langle\infty\rangle$: that is, a single-spin excitation in the middle plane of a magnetic block distinguishes not only $\langle 1\rangle$ from $\langle\infty\rangle$ but also each from $\langle 2\rangle$. Thus, the first-order expansion must potentially consider three coexistence lines. In the event, the

[3] The 12-fold degeneracy of $\langle\infty\rangle$ neither scales with $N$ nor affects the spin–spin correlation function.

three collapse to one. For $z > 0$, all wall phases coexist on the line

$$z = \tfrac{3}{2}(1 - x) \quad (L = 3). \tag{10}$$

For $z > (3/2)(1 - x)$, the $\langle 1 \rangle$ phase has the lowest free energy, while for smaller $z$, the $\langle \infty \rangle$ phase has the lowest free energy.

## 4. Expansion to higher orders

The hierarchy of potential phases in the low-temperature expansion has been described well elsewhere [7, 8, 12, 32] and so will only be summarized. At any order of the expansion, a coexistence region has been established between two 'parent' phases and infinitely many other wall states. (In figure 1 for $L = 4$, this region is the zig-zag line, on which, to first order, parents $\langle 1 \rangle$ and $\langle \infty \rangle$ coexist with all other wall states.) Spin excitations to this order of the expansion cannot distinguish the parents from the other wall states, but by adding some number of additional spin excitations, linked to those of the given order, we can distinguish the two parents from a 'child' phase made by concatenating one period of each parent. As examples, the child of $\langle 1 \rangle$ and $\langle \infty \rangle$ is $\langle 2 \rangle$, while that of $\langle 1 \rangle$ and $\langle 2 \rangle$ is $\langle 12 \rangle$. A connected chain of spin excitations can 'see' the presence or absence of walls over its length; viewed another way, this leads to an effective long-range interaction between walls.

While in principle one could continue the enumeration of connected excitations of two, three and more spins along the lines of table 1, a transfer-matrix technique [11, 2] is well suited to computer symbolic algebra. We defer implementation details to the appendix. The matrices are more involved than those in [2], so the results are for specific cases, from which we conjecture generalizations.

In first order, we have already seen the two-dimensional multiphase region shrink to one dimension (figure 1). We wish to find out whether the line shrinks further to a point or set of points, or whether the line, or a portion of the line, behaves like a multiphase point, with the additional degree of freedom essentially irrelevant. It is also of interest whether all wall states descending from $\langle 1 \rangle$ and $\langle \infty \rangle$ attain stability or only a subset.

We carried out the low-temperature expansion for magnetic blocks of length $L$ between 3 and 17; except for the interesting case of $L = 4$, the hierarchy terminates after just a few phases. Aside from $\langle \infty \rangle$, the only stable phases found for $L = 4$ were of the form $\langle 1^k 2 \rangle$, $0 \leqslant k \leqslant 27$ (the highest calculated) and $k = \infty$ (i.e., $\langle 1 \rangle$). This resembles the ANNNI model [7, 8] more than some clock models in that there do not exist two phases[4] *all* of whose progeny attain stability. Villain and Gordon [33] (see also [9]) distinguish a Devil's staircase [34] from a 'harmless' one. In both, a multiphase point gives rise to a large number of phases that approaches infinity at $T \to 0$. However, in the latter case, at any *finite* $T > 0$, it is argued that only finitely many phases are stable. Since our model fails to find an infinite hierarchy of 'mixed phases' [12], we conjecture that our staircase may similarly be harmless.

The way the $\langle 1 \rangle$-$\langle \infty \rangle$ coexistence line breaks up for $L = 4$ is also of interest. It intersects the multiphase triangle (figure 1) for $1/3 \leqslant z \leqslant 13/9$; outside this region, it ceases to describe coexistence of *ground* states. The symbolic transfer-matrix calculation finds that $\langle 2 \rangle$ is stable on the line only for $3/4 \leqslant z \leqslant 13/9$. Below $3/4$, there is a first-order phase transition between $\langle 1 \rangle$ and $\langle \infty \rangle$. The phase $\langle 12 \rangle$ is stable at $z = 3/4$ and then again for $11/9 \leqslant z \leqslant 13/9$. All subsequent phases $\langle 1^k 2 \rangle$ for which we were able to extract symbolic results ($k \leqslant 5$) are stable for $11/9 < z \leqslant 13/9$ (that is, $3/4$ and $11/9$ drop out). Numerically, $k = 6$–$27$ is stable for $11/9 \lesssim z \leqslant 13/9$, the '$\lesssim$' indicating the inability of the numerical code to distinguish between

[4] $\langle 23 \rangle$ and $\langle \infty \rangle$ in the bulk model [2].

the proper and improper inequality. We conjecture that $\langle 1^k 2\rangle$ is stable for $11/9 \leqslant z \leqslant 13/9$ for all $k \geqslant 2$ and that 'mixed phases' never come in, something we were able to confirm up to the mixed phase $\langle 1^{18}21^{17}2\rangle$.

For $L = 3$, the coexistence line (10) intersects with the region in which wall states have the lowest energy for $0 \leqslant z \leqslant 1$. The states $\langle 1\rangle$, $\langle\infty\rangle$, $\langle 2\rangle$, $\langle 12\rangle$ and $\langle 3\rangle$ are stable on this line segment, but no other phases.

For $L = 5$, the coexistence line is again (9), which passes through the wall-state region for $0 \leqslant z \leqslant 13/9$. The same phases are stable as for $L = 3$: $\langle 2\rangle$ for $0 < z \leqslant 3/4$, $\langle 12\rangle$ for $0 < z \leqslant 3/4$ and $\langle 3\rangle$ for $0 < z < 3/4$. For $L = 6$, the $\langle 1\rangle$-$\langle\infty\rangle$ coexistence line gives the lowest energy for $0 \leqslant z < 13/9$; however, the only other stable phase is $\langle 2\rangle$, and only at the single point $z = 3/4$.

The following pattern appears to hold for $L > 6$: the coexistence line (9) intersects with the wall-state region for $0 \leqslant z \leqslant 13/9$. Even values of $L$ (we computed 8, 10, 12, 14 and 16) give a first-order transition between $\langle 1\rangle$ and $\langle\infty\rangle$ all along the coexistence line. No other phases are stable. For odd $L$ (7, 9, 11, 13, 15 and 17), the phases $\langle 2\rangle$, $\langle 12\rangle$ and $\langle 3\rangle$ are also stable for $0 < z < 3/4$.

## 5. Implications

The low-temperature expansion applies at infinitesimal temperature, but the bulk model has also been investigated with a mean-field theory [12], which should be valid only at high temperature. The low-order phases predicted by the low-temperature expansion were seen to spread out from the multiphase point as temperature increased (figure 2); the only notable discrepancy between the two extreme theories was the presence of phases $\langle 2^k 3\rangle$ in the mean-field calculation, and this was explained in terms of a competing phase. Near the zero-temperature multiphase point, which in the $L = 4$ model would be replaced by the multiphase zig-zag line of figure 1, the spin–spin correlation length is expected to be small, as a large number of commensurate phases with different periods coexist. At any temperature greater than zero and less than the Curie temperature, only one phase is stable; however, in an experimental system, interfacial roughness and interdiffusion might lead to coexisting commensurate phases from nearby points in the temperature-phase space. As the temperature increases, the volumes of stability do as well, so that no phases lie nearby, thus stabilizing a single phase.

Interestingly, the coherence lengths $\xi$ of the basal-plane holmium moments in Ho/Er superlattices have been found to *increase* with temperature $T$ between 8 K and 100 K [35]. Since Er acquires a moment below 100 K, the experimental system is considerably more complex than our simple model; moreover, too few temperatures were measured to permit a comparison to the plateaux one would expect in $\xi(T)$ from figure 2. A similar effect is observed in Er/Lu [36, 23].

The question of commensurate versus incommensurate magnetic modulation also awaits experimental resolution. In the low-temperature expansion, incommensurate phases are only approached, as the limit of a hierarchy of commensurate phases, while the bulk mean-field calculation (figure 2) suggests that these limiting phases will occupy a volume of measure zero in the phase diagram. While several rare-earth systems unambiguously show commensurate phases [29, 20, 36], other superlattices appear to show a continuous increase with temperature in the average turn angle per atomic layer, suggesting that incommensurate phases are generic [1, 37]. We cannot rule out an averaging effect being responsible, but this would appear inconsistent with the absence of plateaux and the expectation of vanishing measure for high-order phases. It will be particularly interesting to investigate whether a statistical-mechanical

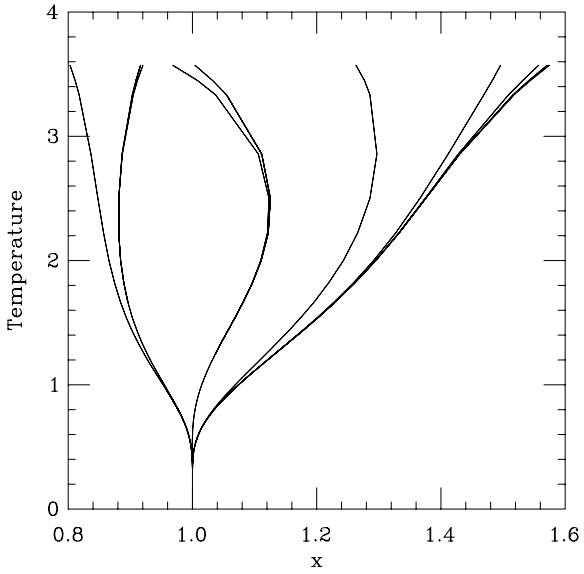


**Figure 2.** Diagram of a hierarchy of phases emanating from a multiphase point at zero temperature up to a Curie temperature. The horizontal axis represents a ratio $x$ of coupling strengths, which at 1 leads to zero-temperature disorder. Raising the temperature from the vicinity of $x = 1$ gives a succession of stable phases. Adapted from figure 1 of [2], where it shows a numerical mean-field calculation on the bulk six-state clock model. In the present context, it can be thought of as schematic for the $T > 0$ behaviour of the system of figure 1 at some point along the zig-zag line, where $x$ represents a transverse dimension.

model not much more complex than that considered here can incorporate more of the qualitative behaviour seen in rare-earth superlattices.

We have shown that a superlattice of helimagnetic and non-magnetic layers exhibits behaviour different from that of the bulk six-state clock model [2]. There are multiphase regions, rather than a single multiphase point. When precisely four magnetic layers lie between non-magnetic spacers, a line segment in the multiphase triangle appears to support a set of phases more like that in the ANNNI model [7, 8] than like the bulk six-state clock model. For other values of $L$, the low-temperature expansion finds only a few stable phases. This raises the interesting experimental question of whether rich magnetic phase diagrams in artificial superlattices could appear for certain magic spacings while being absent for others. If the phase diagram were to depend as sensitively on $L$ as in our model, it might be difficult to grow films sufficiently uniform to test the hypothesis; however, if the extent of the magic coupling were broader (say, $L = 4$–6), the effect could be observable. Further, a multiphase region of coupling space might be more amenable to experiment than a multiphase point that requires exact tuning; such a region, however, would need to have the full dimensionality of the coupling space, something we have not yet constructed.

## Acknowledgment

DAR is a Cottrell scholar of Research Corporation, which has supported this research. We also acknowledge Roxane Rokicki's assistance at an early stage of this work. Calculations were performed at the Research Computing Core Facility at the University of South Florida.

## Appendix

In order to calculate the free-energy difference of a child from its parents, we adapt the transfer-matrix technique [11, 10, 2] to the region with only type-3 walls. We begin in a region over which, to the order already calculated in the low-temperature expansion, parent phases $\langle a\rangle = \langle a_1 a_2 \ldots\rangle$ of period $p_a = \sum_i a_i$ and free energy per spin $f_a$ and $\langle b\rangle = \langle b_1 b_2 \ldots\rangle$ of period $p_b = \sum_i b_i$ and free energy per spin $f_b$ coexist and have lower free energies than their parent phases[5]. We then seek the double free-energy difference

$$a_{\langle ab\rangle} = f_{\langle ab\rangle} - \frac{p_a}{p_a + p_b} f_{\langle a\rangle} - \frac{p_b}{p_a + p_b} f_{\langle b\rangle} \tag{A.1}$$

to leading order. If $a_{\langle ab\rangle} < 0$, the child phase $\langle ab\rangle$ acquires a region of stability. Isolated spin rotations (as in table 1) cannot determine the sign of (A.1), since the three phases, $\langle a\rangle$, $\langle b\rangle$ and $\langle ab\rangle$, have the same free energies to first order. We must consider connected spin excitations: in general, the Boltzmann weight of two (or more) spin rotations that share an axial bond will differ from the weight of the same rotations situated in their respective planes such that they do not share a bond. Since the $J_0$ (in-plane) bond is assumed the most expensive to break, the shortest excitation that distinguishes $\langle ab\rangle$ from its parents provides the leading term in the low-temperature expansion. This requires that the connected excitation should span $(p_a + p_b - 1)$ blocks of length $L$, in the sense that bonds on each end extend through the terminating spacer layers and so sense whether these spacers coincide with walls. The transfer-matrix technique keeps track of all the combinations of connected and disconnected excitations of this length.

As in [2], two cases arise. When the product $(p_a + p_b - 1) \cdot L$ is odd, an excitation of connected spins every second layer distinguishes the child from the two parents, and $2 \times 2$ matrices suffice. When the product is even, we shall need $4 \times 4$ matrices.

The principles are best illustrated by an example. Consider distinguishing $\langle 2\rangle$ from its parents $\langle\infty\rangle$ and $\langle 1\rangle$ when $L = 5$. In the following diagram showing just over one period of the $\langle 2\rangle$ phase, $S$ represents a magnetic layer, while $\hat{S}$ represents a magnetic layer with a flipped spin:

$$S\,\|\,|\,S\hat{S}S\hat{S}S\,\|\,SSSSS\,\|\,|\,S. \tag{A.2}$$

In the $\langle 2\rangle$ phase, the two extremal spacers ($\|$) coincide with walls. In the $\langle 1\rangle$-phase parent, all three spacers coincide with walls, while in the $\langle\infty\rangle$-phase parent, there are no walls. The pictured connected spin excitations, spanning $p_{\langle 1\rangle} + p_{\langle\infty\rangle} - 1 = 1$ block, is the shortest that is possible for $\langle 2\rangle$ but impossible for either parent.

The energy difference (A.1) subtracts from the free energy of diagram (A.2) the parent-diagram free energies. We accomplish this with a product of vectors (lowercase Greek letters) and matrices. For this example, we get

$$a_{\langle 2\rangle} \propto (\beta^\dagger - \alpha^\dagger)\mathcal{A}(\alpha - \beta), \tag{A.3}$$

where $\alpha$ represents a diagram $S\hat{S}S\,\|\,S$, $\beta$ the diagram $S\hat{S}S\,\|\,|\,S$ and $\mathcal{A}$ the diagram $S\hat{S}S\hat{S}S$. The duality operator, defined for vectors by $v^\dagger = (Qv)^T$, with $Q$ having $-1$ all along the antidiagonal, describes the reversed diagram, e.g., $\alpha^\dagger = S\,\|\,S\hat{S}S$, with the clock directions also reversed. Since the spin in an excitation can be rotated 60° counterclockwise (+) or clockwise (−), both conditions must be accounted for. The four entries of a matrix stand for the four ways the two connected spins in a matrix diagram can be flipped:

$$\begin{pmatrix} +- & ++ \\ -- & -+ \end{pmatrix}. \tag{A.4}$$

[5] The period of $\langle\infty\rangle$, for the purpose of (A.1), is 1.

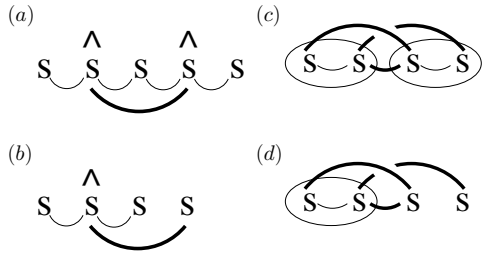


**Figure A1.** A matrix element represents two flipped spins, a vector element one. Boldface bonds are counted at full strength in the Boltzmann weights, while each of the other bonds is counted in two different diagrams and so comes in at half strength. (*a*) A $2 \times 2$ matrix represents flipped spins ($\hat{S}$) in the second and fourth planes. (*b*) A (column) 2-vector contracts with a $2 \times 2$ matrix to its left. (*c*) A $4 \times 4$ matrix represents a flipped spin in one (and only one) of the first two layers and in one (and only one) of the second two. (*d*) A (column) 4-vector contracts with a $4 \times 4$ matrix to its left. (Adapted from [2].)

The entries of a row vector are $(+-)$, those of a column vector $\binom{-}{+}$, so that each contraction in a matrix product sums over the possibilities for a single spin. Each $2 \times 2$ matrix entry gives Boltzmann weights for connected and disconnected combinations of the two constituent spins, as illustrated in figure A1(*a*).

In addition, each matrix entry is a difference between the connected Boltzmann factor and the disconnected factor, as specified by the linked-cluster theorem (6). Vectors terminate the product (figure A1(*b*)). The following $2 \times 2$ matrices are required; common factors of $q^t$ are omitted, since only the signs of the matrix products in the zero-temperature limit matter.

$$S\hat{S}S\hat{S}S \qquad \mathcal{A} = r\begin{pmatrix} 1-r^{x} & r^{3x}-r^{4x} \\ 1-r^{-2x} & 1-r^{x} \end{pmatrix} \tag{A.5}$$

$$S\|\hat{S}S\hat{S}S \qquad \mathcal{B} = \begin{pmatrix} r^{z}-r^{x+z} & r^{z}(r^{3x}-r^{4x}) \\ r^{\frac{3}{2}-\frac{z}{2}}(1-r^{-2x}) & r^{\frac{3}{2}-\frac{z}{2}}(1-r^{x}) \end{pmatrix} \tag{A.6}$$

$$S\hat{S}\|S\hat{S}S \qquad \mathcal{C} = r^{z}\begin{pmatrix} r^{\frac{3}{2}-\frac{3z}{2}}(1-r^{z}) & r^{\frac{3}{2}+\frac{3z}{2}}(1-r^{z}) \\ 1-r^{-2z} & 1-r^{z} \end{pmatrix} \tag{A.7}$$

$$S\|\,|\hat{S}S\hat{S}S \qquad \mathcal{D} = r^{\frac{z}{2}}\begin{pmatrix} 1-r^{x} & r^{3x}-r^{4x} \\ r^{\frac{3}{2}(1-z)}(1-r^{-2x}) & r^{\frac{3}{2}(1-z)}(1-r^{x}) \end{pmatrix} \tag{A.8}$$

$$S\hat{S}\|\,|S\hat{S}S \qquad \mathcal{E} = r^{\frac{z}{2}}\begin{pmatrix} r^{\frac{3}{2}(1-z)}(1-r^{2z}) & r^{\frac{3}{2}(1-z)}(r^{3z}-r^{2z}) \\ r^{3z}-r^{2z} & 1-r^{2z} \end{pmatrix} \tag{A.9}$$

$$S\hat{S}S\|S \qquad \alpha = r^{\frac{1}{2}}\begin{pmatrix} r^{2z} \\ r^{-z} \end{pmatrix} \tag{A.10}$$

$$S\hat{S}S\|\,|S \qquad \beta = r^{\frac{1}{2}}\begin{pmatrix} r^{z} \\ r^{z} \end{pmatrix}. \tag{A.11}$$

The following environments occur only when $L = 3$:

$$S\|\,|\hat{S}S\hat{S}\|\,|S \qquad \mathcal{F} = \begin{pmatrix} r^{\frac{1}{2}-\frac{z}{2}}(1-r^{x}) & r^{3x+z-1}(1-r^{x}) \\ r^{2-2z}(1-r^{-2x}) & r^{\frac{1}{2}-\frac{z}{2}}(1-r^{x}) \end{pmatrix} \tag{A.12}$$

$$S\|\,|\,\hat{S}S\hat{S}\,\|\,S \qquad \mathcal{G} = \begin{pmatrix} r^{\frac{1}{2}}(1-r^x) & r^{-1+3x+\frac{3z}{2}}(1-r^x) \\ r^{2-\frac{3z}{2}}(1-r^{-2x}) & r^{\frac{1}{2}}(1-r^x) \end{pmatrix} \tag{A.13}$$

$$S\,\|\,\hat{S}S\hat{S}\,\|\,S \qquad \mathcal{H} = \begin{pmatrix} r^{\frac{1}{2}+\frac{z}{2}}(1-r^x) & r^{3x+2z-1}(1-r^x) \\ r^{2-z}(1-r^{-2x}) & r^{\frac{1}{2}+\frac{z}{2}}(1-r^x) \end{pmatrix}. \tag{A.14}$$

When $(p_a + p_b - 1)\cdot L$ is even, there is no unique shortest leading-order diagram on the model of (A.2). Rather, a family of such diagrams with flipped spins every second layer except for one pair of axially adjacent flipped spins all span the requisite distance. To account for a single adjacent pair anywhere along the length of an excitation, Seno *et al* [2] introduced $4 \times 4$ transfer matrices of the form

$$\begin{pmatrix} +0+0 & +0-0 & +00+ & +00- \\ -0+0 & -0-0 & -00+ & -00- \\ 0++0 & 0+-0 & 0+0+ & 0+0- \\ 0-+0 & 0--0 & 0-0+ & 0-0- \end{pmatrix}, \tag{A.15}$$

each entry of which considers four adjacent planes in which a spin has rotated in the positive (+) or negative (−) clock direction, or not rotated at all (0). See figure A1(*c*). The four entries of the upper-right quadrant contain no connected spin excitations and so vanish. End-cap vectors (figure A1(*d*)) account for the final pair of planes, one of which will contain a spin flip. The following matrices and end-cap vectors result (again, the common factor of $q^t$ is omitted):

$$\widehat{S\hat{S}S\hat{S}} \quad A = \begin{pmatrix} r(1-r^x) & r^{-\frac{1}{2}}(r^{3x}-r^{4x}) & 0 & 0 \\ r^{\frac{5}{2}}(1-r^{-2x}) & r(1-r^x) & 0 & 0 \\ r^{\frac{1}{2}+x}(1-r) & r^{4x}(r^2-1) & r(1-r^x) & r^{-\frac{1}{2}}(r^{3x}-r^{4x}) \\ r^{-2x}(r^2-r^3) & r^{\frac{1}{2}+x}(1-r) & r^{\frac{5}{2}}(1-r^{-2x}) & r(1-r^x) \end{pmatrix} \tag{A.16}$$

$$\widehat{S\hat{S}S\|\,S} \quad B = \begin{pmatrix} r^{\frac{3}{2}-\frac{z}{2}}(1-r^x) & r^{z-\frac{3}{2}}(r^{3x}-r^{4x}) & 0 & 0 \\ r^{3-\frac{z}{2}}(1-r^{-2x}) & r^z(1-r^x) & 0 & 0 \\ r^{\frac{3z}{2}-x}(r-r^2) & r^{2x+3z}(r-r^{-1}) & r^z(1-r^z) & r^{\frac{5z}{2}}-r^{\frac{7z}{2}} \\ r^{-\frac{3z}{2}-x}\left(r^{\frac{5}{2}}-r^{\frac{7}{2}}\right) & r^{2x}\left(r^{-\frac{1}{2}}-r^{\frac{1}{2}}\right) & r^{\frac{3}{2}+z}(1-r^{-2z}) & r^{\frac{3}{2}-\frac{z}{2}}(1-r^z) \end{pmatrix} \tag{A.17}$$

$$\widehat{S\hat{S}}\,\|\,\widehat{S\hat{S}} \quad C = \begin{pmatrix} r^{2z-1}(1-r^z) & r^{\frac{1}{2}}(r^{2z}-r^{3z}) & 0 & 0 \\ r^{\frac{1}{2}}(r^{2z}-1) & r^2(r^{-z}-1) & 0 & 0 \\ r^{\frac{1}{2}+z}(1-r^z) & r^{2+2z}(r^{2z}-1) & r^{2-z}(1-r^z) & r^{\frac{1}{2}+2z}(1-r^z) \\ r^{z-1}(1-r^z) & r^{\frac{1}{2}+z}(1-r^z) & r^{\frac{1}{2}+2z}(1-r^{-2z}) & r^{2z-1}(1-r^z) \end{pmatrix} \tag{A.18}$$

$$\widehat{S\hat{S}S\|\,|\,S} \quad D = \begin{pmatrix} r^{\frac{3}{2}-z}(1-r^x) & r^{\frac{z}{2}-\frac{3}{2}}(r^{3x}-r^{4x}) & 0 & 0 \\ r^{3-z}(1-r^{-2x}) & r^{\frac{z}{2}}(1-r^x) & 0 & 0 \\ r^{-x}(r-r^2) & r^{\frac{3z}{2}+2x}(r-r^{-1}) & r^{\frac{z}{2}}(1-r^{2z}) & r^z(r^z-1) \\ r^{-x}\left(r^{\frac{5}{2}}-r^{\frac{7}{2}}\right) & r^{2x+\frac{3z}{2}}\left(r^{-\frac{1}{2}}-r^{\frac{1}{2}}\right) & r^{\frac{3}{2}+\frac{5z}{2}}(r^z-1) & r^{\frac{3}{2}-z}(1-r^{2z}) \end{pmatrix} \tag{A.19}$$

$$\widehat{S\hat{S}}\,\|\,|\,\widehat{S\hat{S}} \quad E = \begin{pmatrix} r^{z-1}(1-r^{2z}) & r^{\frac{1}{2}}(r^z-1) & 0 & 0 \\ r^{\frac{1}{2}+3z}(r^z-1) & r^{2-2z}(1-r^{2z}) & 0 & 0 \\ r^{\frac{1}{2}+2z}(1-r^{-z}) & r^{2-z}(1-r^{-z}) & r^2(r^{-2z}-1) & r^{\frac{1}{2}}(r^z-1) \\ r^{2z-1}(1-r^{2z}) & r^{\frac{1}{2}+2z}(1-r^{-z}) & r^{\frac{1}{2}+3z}(r^z-1) & r^{z-1}(1-r^{2z}) \end{pmatrix} \tag{A.20}$$

$$\widehat{SS}\,\|\,SS \qquad a = \begin{pmatrix} r^{2z-\frac{1}{2}} \\ r^{1-z} \\ r^{1+z} \\ r^{z-\frac{1}{2}} \end{pmatrix} \tag{A.21}$$

$$\widehat{SS}\,\|\,|\,SS \qquad b = \begin{pmatrix} r^{z-\frac{1}{2}} \\ r^{1+z} \\ r^{1-z} \\ r^{2z-\frac{1}{2}} \end{pmatrix}. \tag{A.22}$$

A straightforward computer algorithm generates the relevant sequence of matrices; as one example, for $L = 4$,

$$a_{\langle 23\rangle} = (-a^{\dagger} + b^{\dagger})ACAEACA(a - b). \tag{A.23}$$

The program expands and symbolically determines the leading behaviour of $a$ in the zero-temperature limit; if $a$ is negative, the child attains a region of stability with respect to its parents. For sufficiently long chains of matrices, it was impractical to expand the matrix products, and a numerical approach was substituted.

## References


[1] Jehan D A, McMorrow D F, Cowley R A, Ward R C C, Wells M R, Hagmann N and Clausen K N 1993 Magnetic structure of holmium-yttrium superlattices *Phys. Rev.* B **48** 5594–606

[2] Seno F, Rabson D A and Yeomans J M 1993 Low-temperature behaviour of the six-state clock model with competing interactions *J. Phys. A: Math. Gen.* **26** 4887–905

[3] Villain J, Bidaux R, Carton J-P and Conte R 1980 Order as an effect of disorder *J. Physique* **41** 1263–72

[4] Pimpinelli A, Uimin G and Villain J 1991 Ferrimagnetic-helimagnetic transition in an XY magnet with infinitely many phases *J. Phys.: Condens. Matter* **3** 4693–719

[5] Blundell S 2001 *Magnetism in Condensed Matter* (New York: Oxford University Press)

[6] Jensen J and Mackintosh A R 1991 *Rare Earth Magnetism: Structures and Excitations* (New York: Oxford University Press)

[7] Fisher M E and Selke W 1980 Infinitely many commensurate phases in a simple Ising model *Phys. Rev. Lett.* **44** 1502–5

[8] Fisher M E and Selke W 1981 Low temperature analysis of the axial next-nearest neighbour Ising model near its multiphase point *Phil. Trans. R. Soc.* A **302** 1–44

[9] Szpilka A M and Fisher M E 1986 Domain-wall interactions and spatially modulated phases *Phys. Rev. Lett.* **57** 1044–7

[10] Fisher M E and Szpilka A M 1987 Domain-wall interactions. I. General features and phase diagrams for spatially modulated phases *Phys. Rev.* B **36** 644–66

[11] Yeomans J M and Fisher M E 1984 Analysis of the multiphase region in the three-state chiral clock model *Physica* A **127** 1–37

[12] Yeomans J M 1988 The theory and application of axial Ising models *Solid State Phys.* vol 41 (New York: Academic) pp 151–200

[13] Sasaki K 1992 Modulated phases and upsilon points in a spin model with helical ordering *J. Stat. Phys.* **68** 1013–35

[14] Pleimling M, Neubert B and Siems R 1998 Low-temperature phase diagram and critical behaviour of the four-state chiral clock model *J. Phys. A: Math. Gen.* **31** 4871–83

[15] Neubert B, Pleimling M and Siems R 1998 Models for the description of uniaxially modulated materials *Ferroelectrics* **208–209** 141–90

[16] Baibich M N, Broto J M, Fert A, Van Dau F N, Petroff F, Eitenne P, Creuzet G, Friederich A and Chazelas J 1988 Giant magnetoresistance of (001)Fe/(001)Cr magnetic superlattices *Phys. Rev. Lett.* **61** 2472–5

[17] Derbyshire K and Korczynski E 1995 Giant magnetoresistance for tomorrow's hard drives *Solid-State Technol.* **38** 57–66

[18] Araki S, Sano M, Li S, Tsuchiya Y, Redon O, Sasaki T, Ito N, Terunuma K, Morita H and Matsuzaki M 2000 Which spin valve for next giant magnetoresistance head generation? *J. Appl. Phys.* **87** 5377–82

[19] Erwin R W, Rhyne J J, Salamon M B, Borchers J, Sinha S, Du R, Cunningham J E and Flynn C P 1987 Magnetic structure of Dy-Y superlattices *Phys. Rev.* B **35** 6808–25
[20] Borchers J A, Salamon M B, Erwin R W, Rhyne J J, Nieuwenhuys G J, Du R R, Flynn C P and Beach R S 1991 Structural and magnetic properties of Er thin films and Er/Y superlattices: II. Modification of the commensurate spin states *Phys. Rev.* B **44** 11814–24
[21] Swaddling P P, Cowley R A, Ward R C C, Wells M R and McMorrow D F 1996 Magnetic structures of holmium-lutetium alloys and superlattices *Phys. Rev.* B **53** 6488–98
[22] Bruno P 1995 Theory of interlayer magnetic coupling *Phys. Rev.* B **52** 411–39
[23] Cowley R A 1998 The coherence of the magnetic structures of rare-earth superlattices *J. Magn. Magn. Mater.* **177–181** 1156–61
[24] Cowley R A 1999 The magnetic interactions in rare-earth metals and superlattices *J. Magn. Magn. Mater.* **196–197** 680–3
[25] Rossat-Mignod J, Burlet P, Bartholin H, Vogt O and Lagnier R 1980 Specific heat analysis of the magnetic phase diagram of CeSb *J. Phys. C: Solid State Phys.* **13** 6381–9
[26] Moudden A H, Moncton D E and Axe J D 1983 Thiourea under a high electric field: x-ray studies *Phys. Rev. Lett.* **51** 2390–3
[27] Durand D, Dénoyer F, Currat R and Vettier C 1984 Neutron-diffraction study of thiourea under high electric field *Phys. Rev.* B **30** 1112–4
[28] Seno F, Yeomans J M, Harbord R and Ko D Y K 1994 Ground state of a model with competing interactions and spin anisotropy *Phys. Rev.* B **49** 6412–5
[29] Bohr J, Gibbs D, Axe J D, Moncton D E, D'Amico K L, Majkrzak C F, Kwo J, Hong M, Chien C L and Jensen J 1989 Diffraction studies of rare earth metals and superlattices *Physica* B **159** 93–105
[30] Redner S 1981 One dimensional Ising chain with competing interactions: exact results and connection with other statistical models *J. Stat. Phys.* **25** 15–23
[31] Wortis M 1974 Linked-cluster expansion *Phase Transitions and Critical Phenonmena* vol 3 ed C Domb and M S Green (New York: Academic) pp 113–80
[32] Yeomans J M 1992 *Statistical Mechanics of Phase Transitions* (New York: Oxford University Press)
[33] Villain J and Gordon M B 1980 The devil's staircase and harmless staircase: I. Oscillating interactions through elastic strains or other harmonic fields *J. Phys. C: Solid State Phys.* **13** 3117–34
[34] Bak P and von Boehm J 1980 Ising model with solitons, phasons, and 'the devil's staircase' *Phys. Rev.* B **21** 5297–308
[35] Simpson J A, McMorrow D F, Cowley R A, Jehan D A, Ward R C C, Wells M R and Clausen K N 1994 Competing anisotropies in holmium-erbium superlattices *Phys. Rev. Lett.* **73** 1162–5
[36] Simpson J A, Cowley R A, Ward R C C, Wells M R and McMorrow D F 1997 The magnetic properties of er/lu superlattices *J. Phys.: Condens. Matter* **9** 8693–705
[37] Cowley R A 2004 Magnetic structures and coherence of rare-earth superlattices *Physica* B **350** 1–10